SECOND EUROPEAN CONFERENCE ON EARTHQUAKE ENGINEERING
AND SEISMOLOGY, ISTANBUL AUG. 25-29, 2014

IMPLICATIONS OF YIELD PENETRATION ON THE REQUIREMENTS FOR CONFINEMENT OF R.C. WALL ELEMENTS

Souzana TASTANI[1] and Stavroula PANTAZOPOULOU[2]

ABSTRACT

Design of walls requires that confinement for curvature ductility in the critical (plastic hinge) regions should extend over a length in the compression zone of the cross section at the wall base where strains in the ULS exceed the limit of 0.0035. However performance of flexural walls in the recent earthquake in Chile (2010) indicates that the actual compression strains developed were higher than estimated, being responsible for several of the reported failures by toe crushing. In this study, the method of estimating the confined region and magnitude of compression strains in slender walls are revisited in order to account for the newly identified kinematic interaction with the lumped rotations that occur at the wall base due to penetration of bar yielding into the supporting anchorage. Design charts estimating the amount of yield penetration in terms of the resulting lumped rotation at the wall base are used to quantify the increased demands for compression strain in the critical section. The estimated strain increase exceeds over 30% of the base value estimated from the existing design expressions, which explains the frequently reported occurrence of toe crushing even in well confined slender walls under high drift demands. Example cases are included in the presentation to illustrate the behavioral parametric trends and implications in seismic design of walls.

INTRODUCTION

The M8.8 Richter earthquake that occurred in February of 2010 in Chile was marked by several wall failures – field observations identified several compression failures particularly in slender walls (in high-rise buildings). This raised some anxiety in the engineering community, following the recent shift to displacement-based design of walls (in EC8-I and ACI318) where confinement requirements are linked to the estimate of compressive strain demand at the wall toe. Thus, success of this approach rides on the dependability of the compression strain estimate. Evidence from the Chile failures suggests that strains well beyond the spalling / crushing limit of unconfined concrete developed during this M8.8 Richer earthquake.

Further evidence resulting from comparison between analytical with experimental values of compressive strain in reinforced concrete shear walls bent in flexure have shown that there is a consistent tendency for underestimation of deformations. Several experimental studies point to a higher than estimated compressive strain in the compression zone (Hannewald et al., 2012, Wallace et al., 2012). This finding is consistent with the observed compression crushing failures at the base corner of structural walls mentioned in the preceding (Wallace and Moehle, 2012).

Slender walls usually occur in taller structures for which $T_1 > T_C$, and therefore EC8-I assumes that an upper limit to curvature ductility demand μ_ϕ, may be estimated from the behavior factor q through the relationship (equal displacement rule):

[1] Lecturer, Democritus University of Thrace, Xanthi - Greece, stastani@civil.duth.gr
[2] Professor, University of Cyprus, Nicosia-Cyprus, pantaz@ucy.ac.cy

$$\mu_\phi = 2q - 1 \quad (1)$$

where, T_1 is the fundamental period of the building and T_C the period at the upper limit of the constant acceleration region of the total acceleration design spectrum. The external most stressed part of the compression zone of the critical wall section is required to be confined by a mechanical reinforcement ratio, $a \cdot \omega_{wd}$ that exceeds the limit:

$$a \cdot \omega_{wd} \geq 30\mu_\phi(\nu_d + \omega_v) \cdot \varepsilon_{sy,d} \frac{b_w}{b_o} - 0.035 \quad (2)$$

Parameters in Eq. (2) include, the mechanical ratio of vertical web reinforcement, $\omega_v = \rho_v f_{yd,v} / f_{cd}$, and the $_d$ subscript identifies design material values (these are taken equal to the characteristic values for the earthquake combination). Also, b_w is the thickness of the wall section and b_o the width of the confined core in the boundary element of a wall. The length of the wall end that need be confined (confined boundary element) measured from the centroid of the outside stirrup is equal to:

$$l_c = x_u \cdot \left(1 - \frac{\varepsilon_{cu}}{\varepsilon_{cc,u}}\right); \quad \varepsilon_{cc,u} = 0.0035 + 0.1 \cdot a \cdot \omega_{wd} \quad (3)$$

where term ε_{cu} is the strain at compression spalling (taken for simplicity equal to 0.0035) and $\varepsilon_{cc,u}$ the strain capacity of confined concrete. Thus, special transverse reinforcement is required over that part of the compression zone (i.e. l_c) where the compressive strains exceed the crushing strain of unconfined concrete, ε_{cu}=0.0035 (EC8-I, Fig. 1a).

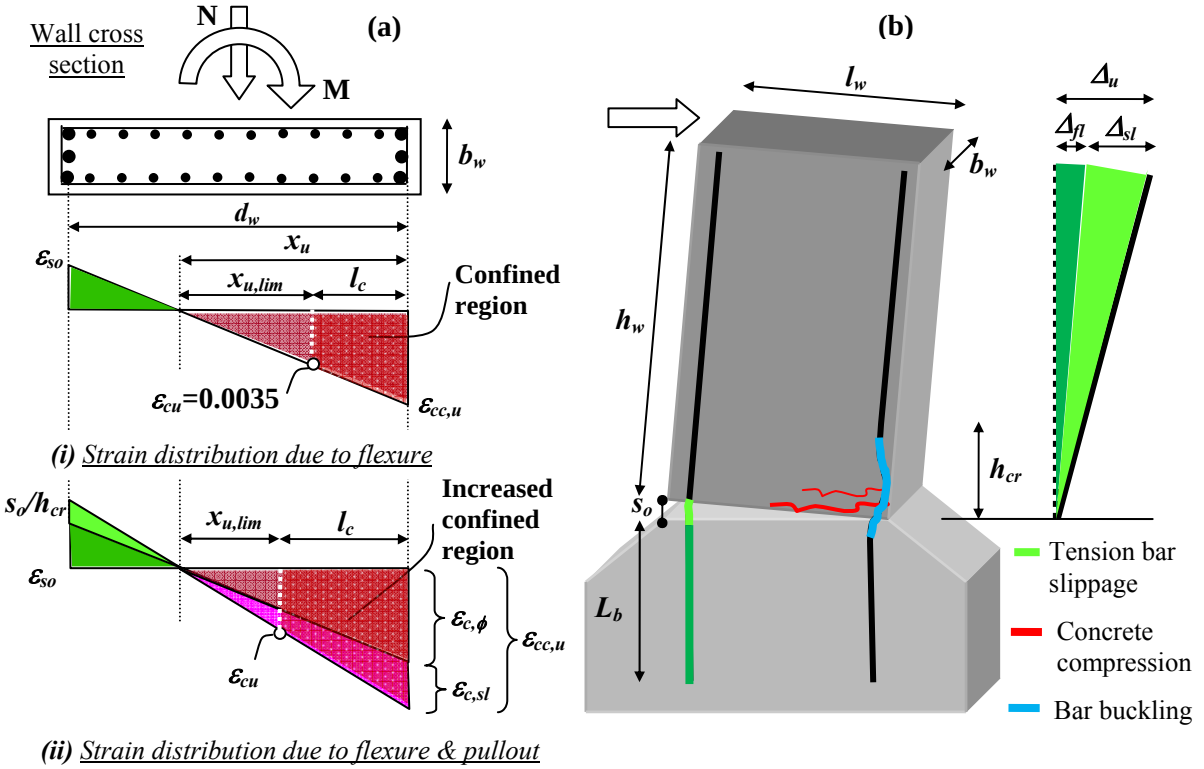

Figure 1. (a) Cross sectional definition of the confined boundary element by considering (i) only flexural response and (ii) flexural and pullout response. (b) Cantilever model for deformation analysis of a shear wall.

According to Eq. (3) the check of the compressive strains along the compressive zone, x_u, is converted to a check for the depth of compression zone against a limiting value, $x_{u,lim}$, associated with attainment of the ε_{cu}=0.0035. The threshold value of $x_{u,lim}$ is defined by Eq. (4) where term θ_{pl} is the local plastic hinge rotation at the wall base, defined as Δ_u/h_w with Δ_u being the total peak displacement

demand (Fig. 1b) for the wall structure, h_w is the wall height (measured from the critical cross-section up to the point of inflection), and h_{cr} is the plastic hinge length (this is the length in the clear height of the wall where yield penetration may occur – and it is generally much lower than the design length of critical region which is used for detailing). For slender walls, h_{cr} is taken up to half the length of the wall cross section, l_w (Wallace and Moehle 2012). Term Δ_u is estimated from the design earthquake (from spectral displacement, S_d, as $\Delta_u = S_d\, C_d$ where S_d is obtained from spectral acceleration S_a, according with, $S_d=S_aT^2/(4\pi^2)$, and C_d is a coefficient around 1.3 required to convert spectral displacement to displacement at the top of the wall structure). In design, the ultimate drift ratio demand is set equal to the local plastic hinge rotation at the wall base, θ_{pl}. The extreme fiber compressive strain $\varepsilon_{cc,u}$, at the critical cross section is obtained as:

$$\left.\begin{aligned} \theta_{pl} &= \frac{\Delta_u}{h_w} = \phi_u \cdot h_{cr} \\ \phi_u &= \frac{\varepsilon_{cc,u}}{x_u} = \frac{0.0035}{x_{u,lim}} = \frac{\mu_\phi \cdot \varepsilon_{sy}}{d_w - x_u} \end{aligned}\right\} \quad \begin{aligned} &\Rightarrow \quad \varepsilon_{cc,u} = \frac{\theta_{pl}}{h_{cr}} \cdot x_u = 2\frac{\Delta_u}{h_w} \cdot \frac{x_u}{l_w} \\ &\Rightarrow \quad x_{u,lim} = 0.0035 \cdot \frac{h_{cr}}{\theta_{pl}} \approx \frac{l_w}{600 \cdot \theta_{pl}} \end{aligned} \tag{4a}$$

Combining Eqs. (2) and (3) regarding the strain $\varepsilon_{cc,u}$ it results:

$$\varepsilon_{cc,u} = 0.0035 + 0.1 \cdot a \cdot \omega_{wd} = \frac{\theta_{pl}}{h_{cr}} \cdot x_u \quad \Rightarrow \quad x_u = \frac{h_{cr}}{\theta_{pl}} \cdot \left(0.0035 + 0.1 \cdot a \cdot \omega_{wd}\right) \tag{4b}$$

Thus, from Eq. (4a) when $x_u > x_{u,lim}$, confined boundary elements are required in the length $l_c=(x_u-x_{u,lim})$. The EC8-I requires that $l_c=x_u-x_{u,lim} \geq \max[0.15l_w, 1.5b_w]$ in order for the wall to provide the required deformation capacity. Also, Eq. (4b) relates the length of the compression zone x_u with the attained plastic hinge rotation and the confinement detailing of the critical cross section. Note here that $l_c=(h_{cr}/\theta_{pl})\cdot(0.1a\omega_{wd})\approx(l_w/\theta_{pl})\cdot(0.05a\omega_{wd})$, therefore, the rotational capacity of the wall, θ_{pl} is limited by the available amount of boundary confinement through the following: $\theta_{pl}=(l_w/l_c)\cdot(0.05a\omega_{wd})$.

KINEMATICS OF YIELD PENETRATION AND PULLOUT ROTATION

Yield penetration is known to destroy interfacial bar – concrete bond allowing unhampered bar slippage. This affects the plastic rotation capacity of the member by increasing the contribution of bar pullout. As a result secondary axial strains are enforced in the compression zone within the plastic hinge region of structural walls, which may be critical in the displacement-based detailing procedures that link confinement of walls to compressive strains (EC8-I).

The compressive strain in the compression zone of shear walls could be increasingly affected by the lumped rotation at the critical cross section near the face of the support due to pullout of the tension reinforcement from its anchorage. In this case damage is concentrated at a single, large crack at the foundation - wall interface (Fig. 2a), where the lumped rotation could account by as much as 75% of the total member rotation (Fig. 2b, Wallace and Moehle, 2012). Because the compression zone cannot penetrate into the support as would be required by the end section rotation (assuming the familiar cantilever model, Fig. 1b), it is forced to undergo increased contraction strain in order to counterbalance the effects of rotation. A kinematic relationship has been proposed by Syntzirma et al. (2010) to account for this compression strain increase, which states that the compressive strain at the extreme fiber of the cross section, $\varepsilon_{cc,u}$, in the plastic hinge region of a flexural member not only depends on the sectional curvature ϕ and the depth of compression zone, x_u, but also on the amount of reinforcement slip, s_o, as follows:

$$\varepsilon_{cc,u} = \varepsilon_{c,\phi} + \varepsilon_{c,sl} = \varepsilon_{so} \cdot \frac{x_u}{d_w - x_u} + \frac{s_o}{h_{cr}} \cdot \frac{x_u}{d_w - x_u} = \left(\varepsilon_{so} + \frac{s_o}{h_{cr}}\right) \cdot \frac{x_u}{d_w - x_u} \tag{5}$$

where, ε_{so} is the axial strain in the tension reinforcement at the critical section, d_w is the effective depth of the wall cross-section (taken here as $0.8l_w$ where l_w is the section length) and x_u is the depth of the compression zone (see Fig. 1a). (When axial load v_d is in the range of 0.1, term x_u is usually less than $0.5l_w$, since, at balanced condition, where tension steel has yielded and the extreme compression strain of concrete is at its ultimate value (0.0035): $x_u=\varepsilon_{cu}/(\varepsilon_{cu}+\varepsilon_{sy})\cdot d_w=0.0035/(0.0035+0.0025)\cdot 0.8l_w=0.47l_w$.)

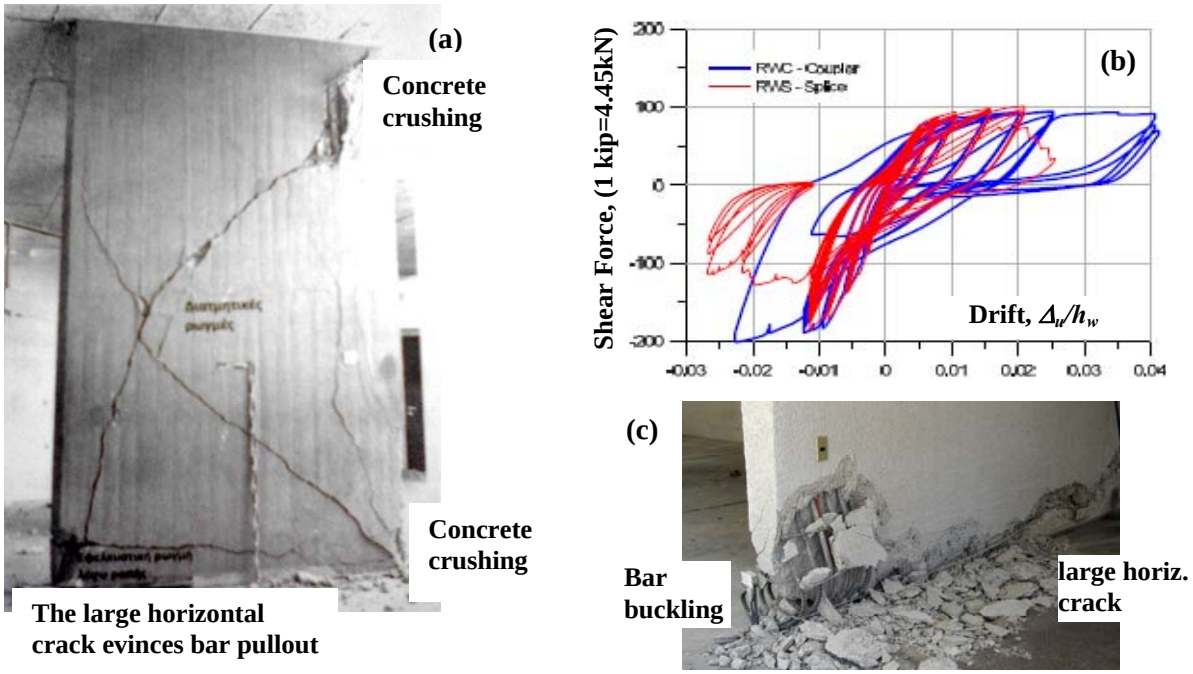

Figure 2. (a) Shear wall failure due to concrete crushing of the cross section compression zone and development of a single wide crack at the foundation-wall interface (Karagiannis 2013). (b) Increased total drift as a result of the lumped rotation due to tension reinforcement pullout from its anchorage (Wallace and Moehle 2012). (c) Buckling of bars due to excessive compression strain induced from tension bar pullout from its anchorage.

A schematic representation of Eq. (5) is shown in Fig. 1(a.ii) where the slip magnitude designated at the critical cross section (Fig. 1b) is divided by the critical plastic hinge length h_{cr} in order to be accounted for as an average axial strain increment in the cross-section (h_{cr} is taken up to half the length of the wall cross section). Note that in design, the plastic hinge length h_{cr} is taken as high as the sectional depth of shear walls in order to enforce greater amounts of detailing in the lower storey of wall-buildings: in these cases the combined action of the relatively high axial load (in the order of v_d=0.4) restrains / delays the tension reinforcement from yielding whereas the confining boundary elements allow the moment capacity to be increased as a result of the confinement provided to the compression concrete; through detailing the objective is to prevent the compression zone from bulging out as shown in Fig. 2(c). Hence, yielding penetrates upwards along the wall if the moment-curvature response exhibits hardening, thereby effectively increasing the plastic hinge length. Equation (5) highlights a newly identified interaction between flexural action and pullout behavior of the reinforcement: evidently, bar slip affects cross sectional equilibrium through the effect it has on strain $\varepsilon_{cc,u}$. Given the cross sectional geometry and the material stress-strain laws, the resulting moment – curvature (M-ϕ) relationship at the critical cross section is no longer unique for a given axial load value, but it depends on the details and the state of stress in the reinforcement anchorage.

Objective of the paper is to identify the practical implications of yield penetration on rotation capacity (i.e. Δ_u) and the associated confinement requirements (i.e. $x_{u,lim}$) of shear walls.

EFFECTS ON COMPRESSION STRAIN DEMAND

To identify the implication that slip of tension reinforcement has on the concrete compressive strain consider as an example a wall cross section having a width b_w=200mm, height l_w=1000mm

(d_w=0.8l_w=800mm), compression zone depth x_u=0.25l_w=250mm, plastic hinge length h_{cr}=0.5l_w and tension reinforcement strain beyond yielding, ε_{so}=0.006. The corresponding value of $\varepsilon_{cc,u}$ is 0.0027 if slip is ignored (i.e. s_o=0 in Eq. 5), but for as small a slip value as s_o=2mm the corresponding concrete strain $\varepsilon_{cc,u}$ is increased to 0.0045, hence the extreme fibers of the compression zone are at a state of delamination and crushing. The increase of compressive strain $\varepsilon_{cc,u}$ in the plastic hinge zone due to anchorage pullout drives the concrete to enter faster in its stress –strain softening branch and if confinement is absent then the longitudinal reinforcement on the compression side is susceptible to imminent bar buckling (Fig. 2c) which is usually accompanied with bar fracture on the tension side (Jiang et al. 2013).

The slippage of the tension reinforcement is also accounted for in the total peak displacement Δ_u by considering that the latter is the sum of the flexural and the pullout contributions, Δ_{fl} and Δ_{sl}, as depicted in Fig. 1b. Thus, the increase of peak displacement due to slippage results in the reduction of $x_{u,lim}$ as per Eq. (4a) and to a commensurate increase of the required confined depth of the shear wall as illustrated in Fig. 1a(ii).

Equation (5) underlines the importance of dependably estimating bar slip, s_o, as a prerequisite to accurately evaluating the state of stress in the critical cross section of shear walls adjacent to monolithic connections. Note that when the bar is strained beyond yielding, a large fraction of the slip measured in tests is owing to inelasticity spreading over the bar anchorage, known as yield penetration.

Calculation of slip in yielding anchorages is essential for accurate interpretation of the reported failures described in the preceding. These implications concern a number of different aspects:

(a) The excessive amount of reinforcement slip from the yielded anchorage increases the flexibility of the member connection to its support, where a large fraction of the rotation is owing to reinforcement pullout from the anchorage rather than flexural curvature over the member length.

(b) The kinematics of rotation due to bar pullout causes increased strains in the compression zone of the member, particularly in the plastic hinge zone h_{cr} adjacent to the support (Fig. 1b). Performance based detailing of certain structural members is controlled by the amount of concrete compression strains (e.g. structural walls, EC8-I and ACI318 Chapter 21). In these cases, the effects of yield penetration may cancel the design objective.

(c) It is shown that yield penetration may limit the strain development capacity of longitudinal reinforcement, an issue that is particularly important in existing construction where either the available anchorage is limited, or, the structural member has undergone yielding during previous seismic events thereby exhausting part of the dependable strain capacity of the anchorage of primary reinforcement. To address these issues the equations for bond of yielding rebars (Tastani and Pantazopoulou, 2013) are applied to explore the bar strain development capacity over yielded anchorages.

BAR ANCHORAGE STRAIN DEVELOPMENT CAPACITY

The solution developed in this section evaluates the strain development capacity of a bar with an idealized bilinear stress-strain curve having a post-yielding hardening slope, E_{sh} (no plateau), anchored in concrete over a length L_b (Fig. 3a); the assumed bond-slip curve has the characteristics depicted in Fig. 3(b). The maximum slip, s_o^{max}, that may be attained by an adequately anchored straight bar at the critical cross section of the shear wall is given by Eq. (6a). It comprises three contributions (Tastani and Pantazopoulou 2013), namely: (i) the slip of the anchorage end point at imminent anchorage failure, that is equal to the slip at the end of the ascending branch of the local bond-slip law, s_1 (Fig. 3a & b), (ii) the slip owing to integration of the linearly varying bar strains - from zero at the anchorage end point, to the yield strain ε_{sy} along the minimum bonded length, $L_{b,min}=D_b/4(f_{sy}/f_b^{max})$ as $1/2\varepsilon_{sy}\cdot L_{b,min}$ (thus $s_2=s_1+1/2\varepsilon_{sy}\cdot L_{b,min}$) and (iii) the slip due to yield penetration over the *maximum sustainable debonded length (MSDL)*, which is estimated from: $\ell_r=(L_b-L_{b,min})$ as $1/2(\varepsilon_{sy}+\varepsilon_{so}^{max})\ell_r$.

$$s_o^{max} = s_1 + \frac{1}{2}L_b\varepsilon_{sy} + \frac{1}{2}\left(L_b - L_{b,min}\right)\cdot\varepsilon_{so}^{max} \tag{6a}$$

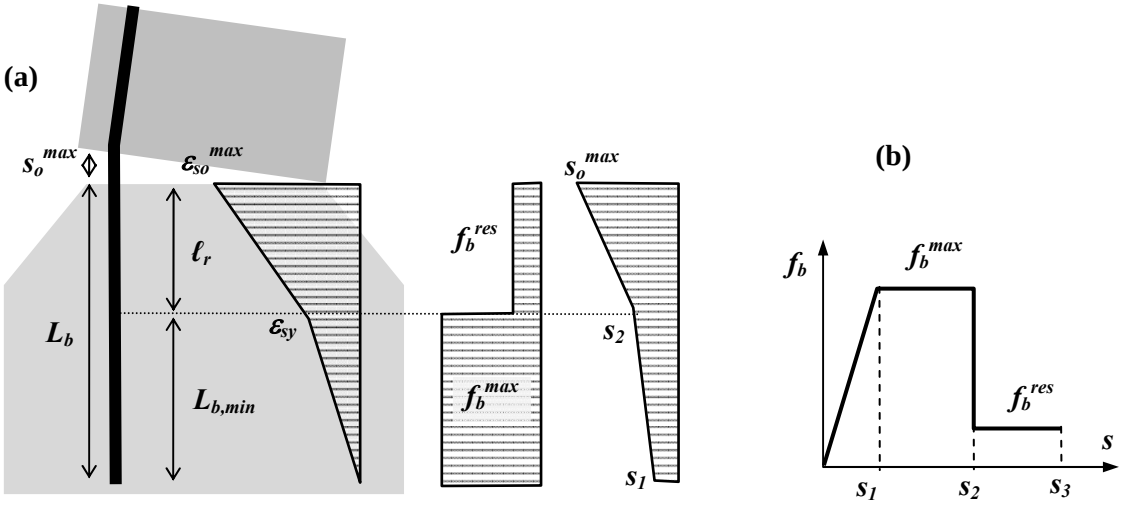

Figure 3. (a) Attenuations of inelastic bar strain capacity and the associated bond stress and slip along the anchorage. (b) Simplified elasto-perfectly plastic with a post-peak residual plateau bond-slip law.

Therefore, the definition of an MSDL is based on the postulate that prior to complete anchorage failure, the bar has become gradually debonded from concrete over the length ℓ_r, so that the residual bonded length is just adequate to develop the bar force as required by equilibrium, and that any further increase in the bar strain at the critical section leads to pullout failure. At that reference point of imminent anchorage failure, the lumped rotation at the base of the wall may be estimated from:

$$\frac{\Delta_{sl}}{h_w} = \frac{s_o^{max}}{d_w - x_u} \tag{6b}$$

The associated tensile strain capacity of the reinforcement, i.e., the maximum strain that may be developed by the anchorage, ε_{so}^{max}, and corresponding bar strain ductility, $\mu_{\varepsilon s}$, are given by Eqs. (7):

$$\varepsilon_{so}^{max} = \varepsilon_{sy} + 4 \cdot \left(L_b - L_{b,min}\right) \frac{f_b^{res}}{D_b E_{sh}} \quad ; \text{Strain ductility: } \mu_{\varepsilon s} = \frac{\varepsilon_{so}^{max}}{\varepsilon_{sy}} = 1 + 4 \cdot \frac{L_b - L_{b,min}}{D_b} \cdot \frac{f_b^{res}}{E_{sh} \cdot \varepsilon_{sy}} \tag{7}$$

Term f_b^{res} is the residual resistance of bond (see the degraded end of the bond-slip law in Fig. 3b), and D_b is the bar diameter.

Table 1. Bond strength values for anchorage pullout failure and $\varepsilon_{so} \leq \varepsilon_{sy}$ (*fib* MC2010)

f_c'(MPa)	12	16	20	25	30
Good bond conditions: $f_b^{max}=2.5\sqrt{f_c'}$(MPa)	8.7	10	11.2	12.5	13.7
All other bond conditions: $f_b^{max}=1.25\sqrt{f_c'}$(MPa)	4.3	5	5.6	6.3	6.8
For *S500* & $D_b \leq 20$mm: $f_{bd}=2 \cdot f_{bo}= =2 \cdot n_1 n_2 n_3 n_4 (f_c'/20)^{0.5}$	2.8	3.2	3.6	4.0	4.4

Equation (7) is investigated below with regards to the important parameters through a sensitivity study. Figure 4a plots the estimated strain ductility capacity $\mu_{\varepsilon s}=\varepsilon_{so}^{max}/\varepsilon_{sy}$ of a straight anchored bar, which can be supported by the normalized anchorage length L_b/D_b, for steel class S500, five different concrete types (f_c' =30MPa, 25MPa, 20MPa, 16MPa and 12MPa), two bond conditions (the characteristic bond strength f_b^{max} was taken equal to $2.5\sqrt{f_c'}$ and $1.25\sqrt{f_c'}$ for good and all other bond conditions respectively, values taken from Table 1 in accordance with *fib* MC2010) and two values for the hardening modulus of steel (1% and 5% of E_s=200GPa). In Fig. 4a the lower the concrete quality, the thinner the line of the corresponding curve. Note that the method to develop such diagrams has been presented elsewhere (Tastani and Pantazopoulou 2013). Similar diagrams to those of Fig. 4a are produced by using the design bond strength f_{bd} (nominal values are included in the fourth line of Table 1 and are calculated as per the *fib* MC2010 through the expression $f_{bd}=2 \cdot f_{bo}= =2 \cdot n_1 n_2 n_3 n_4 (f_c'/20)^{0.5}$)

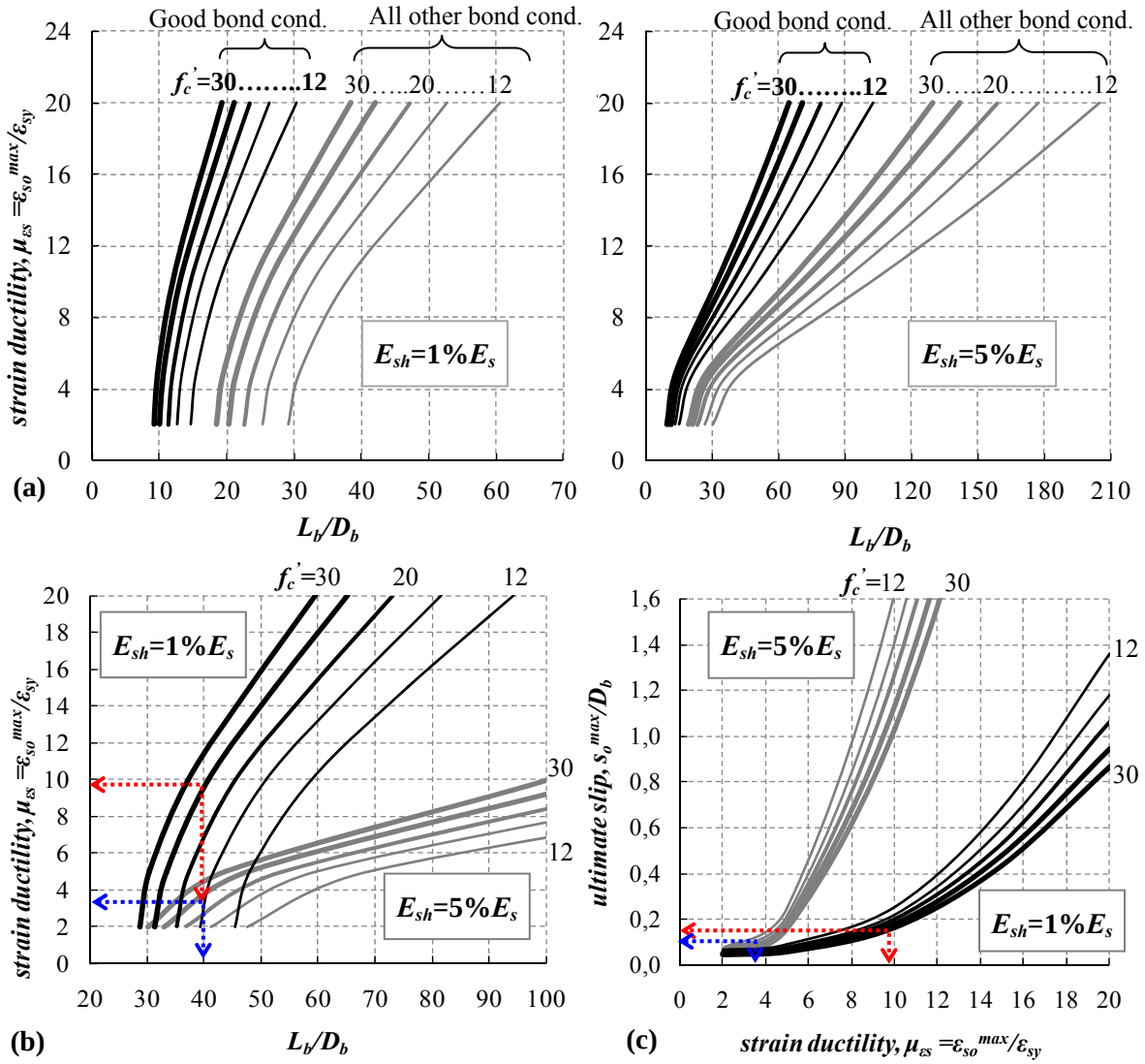

Figure 4. (a) Anchorage strain ductility capacity versus the required anchorage length for steel category **S500**, two values for hardening modulus (E_{sh}**=1%** and **5%**E_s), five concrete strengths (f_c**'=12, 16, 20, 25, 30MPa**) and two bond conditions (see Table 1). When using design bond strength f_{bd} values (4th line of Table 1): (b) diagrams $\mu_{\varepsilon s} - L_b/D_b$ and (c) charts of the ultimate slip as a function of strain ductility capacity.

rather than the characteristic bond strength f_b^{max} (Fig. 4b). Comparing corresponding curves of Figs. 4a,b (with all other variables the same, i.e. E_{sh} and f_c') it becomes clear that **in design** (Fig. 4b), conservatively, the required anchorage length is longer than that calculated by using the characteristic bond strength (Fig. 4a) for the same target strain ductility.

To illustrate the use of Fig. 4 and also the implications of Eq. (7) on **design** issues let us consider a bar at the wall base with yielding stress f_{sy}=500MPa and a hardening modulus E_{sh}=5%E_s, of diameter D_b=20mm, with design bond strength f_{bd}=4MPa (f_c'=25MPa, Table 1) and s_1=0.2mm anchored over a length L_b=800mm (=40D_b>$L_{b,min}$=625mm). In Fig. 4b the grey curve denoted by f_c'*=25MPa* – E_{sh}*=5%*E_s and the chosen anchorage length of L_b/D_b=40 result in a strain ductility capacity of the anchorage equal to $\mu_{\varepsilon s}=\varepsilon_{so}^{max}/\varepsilon_{sy}$=3.5 (see the blue dashed line in Fig. 4b) and thus, the maximum strain development capacity of the reinforcement is limited to: $\varepsilon_{so}^{max}\approx$0.009, which is lower than the design ultimate strain of the reinforcement (ε_{ud}=0.02) and far less than the nominal rupture strain of the material (ε_{uk}=0.075 for class C, EC2 2004). The associated slip calculated through Eq. (6) is $s_o^{max}\approx$2mm (or 0.1D_b - see the blue dashed line in Fig. 4c) whereas the lumped drift is in the order of 0.36% (d_w=800mm, and x_u=250mm).

Equation (5) is used twice with the cross section data of the previous example: once without and once with due consideration of the slip magnitude. These two alternatives result in a maximum confined strain demand of $\varepsilon_{cc,u}(s=0)=0.004$ and $\varepsilon_{cc,u}(s=s_o^{max})=0.005$ respectively – that is an increase by 20% in the value of peak compressive strain. For the same anchorage details, but using steel with milder strain hardening (thus $E_{sh}=1\%E_s$, see the black curves in Fig. 4b) the corresponding steel strain ductility magnitudes are $\mu_{\varepsilon s}=\varepsilon_{so}^{max}/\varepsilon_{sy}=9.5$ (see the red dashed line), and thus, the strain development capacity of the reinforcement is now, $\varepsilon_{so}^{max}=0.024$, with $s_o^{max}\approx 3.3$mm (or $0.16D_b$ - see the red dashed line in Fig. 4c) and the corresponding confined concrete strain demands equal to $\varepsilon_{cc,u}(s=0)=0.011$, $\varepsilon_{cc,u}(s=s_o^{max})=0.013$. This highlights the significance that steel properties may have on the available deformation capacity of the anchorage. (Note that one could approximate the results of the preceding analysis without the charts of Fig. 4, by only considering values for f_b^{max}, f_b^{res}, s_1 and E_{sh} in Eqs. 6-7.)

The result of the first example, where $E_{sh}=5\%E_s$, is interpreted as follows: Whereas the anchorage length suffices for the bar to develop its yielding strength however it imposes (a) limitations regarding the available bar strain development capacity and the flexural ductility of the structural element, and (b) this finding has implications on the hierarchy of failure modes of the wall cross section by seriously increasing the imposed compressive strain demands in the confined region.

DUCTILE ROTATION CAPACITY ASSOCIATED WITH THE ANCHORAGE DEFORMATION CAPACITY

In design, the ultimate drift ratio demand is set equal to the local plastic hinge rotation at the wall base, θ_{pl}. Thus, it may be shown through the kinematics of the deformed member and the concrete mechanics that the term θ_{pl} comprises flexural and pullout (slip) components. Thus, $\Delta_u=\Delta_{fl}+\Delta_{sl}$ in Fig. 1b where, according with Eq. 6b:

$$\theta_{pl}=\frac{\Delta_u}{h_w}=\frac{\Delta_{fl}}{h_w}+\frac{\Delta_{sl}}{h_w}=\phi_u\cdot h_{cr}+\frac{s_o^{max}}{d_w-x_u} \tag{8}$$

The cross sectional curvature, ϕ_u, is analyzed considering the anchorage tensile strain capacity of the reinforcement ε_{so}^{max} (which is a unique magnitude), leading to Eq. (8a). But if ϕ_u is obtained by considering the increased concrete compressive strain through Eq. (5) then the ultimate drift is doubly affected by the bar slippage, as shown by Eq. (8b). Note that Eqs. (5) are applicable under the requirement that the anchorage is able to develop its strain capacity ε_{so}^{max} prior to the occurrence of other, competing modes of failure (e.g. bar buckling, shear failure, limiting flexural failure).

$$\theta_{pl}(\varepsilon_{so})=\frac{\varepsilon_{so}^{max}}{d_w-x_u}h_{cr}+\frac{s_o^{max}}{d_w-x_u} \tag{8a}$$

$$\theta_{pl}(\varepsilon_{cc,u})=\frac{\varepsilon_{cc,u}}{x_u}h_{cr}+\frac{s_o^{max}}{d_w-x_u}\quad\overset{Eq.(5)}{\Rightarrow}\quad\theta_{pl}(\varepsilon_{cc,u})=\frac{\varepsilon_{so}^{max}}{d_w-x_u}h_{cr}+2\frac{s_o^{max}}{d_w-x_u} \tag{8b}$$

To illustrate the impact of bond response (through the strain capacity ε_{so}^{max} and the associated slip s_o^{max} originating at the critical cross section where the wall is connected with the pedestal) on the attained ultimate drift ratio defined by Eq. (8b) the following parametric study is presented through the diagrams of Fig. 5. For two common cross section lengths (i.e. $l_w=1000$ and 3000mm) and for five levels of compression zone depths (i.e. $x_u=0.1$, 0.2, 0.3, 0.4 and 0.5 of l_w where the thinner the curve the lower the x_u value in Fig. 5). Material properties were, $f_c'=25$MPa and $E_{sh}=1\%E_s$, with a nominal design bond strength value as listed in the 4th line of Table 1 (Fig. 4b). The produced diagrams correlate the ultimate drift ratio with the strain ductility capacity of the anchorage and the mechanical confinement reinforcement ratio of the section, $a\cdot\omega_{wd}$. The following points are deduced:

(i) For a constant depth of compression zone after reinforcement yielding (e.g. here, $x_u=0.4l_w$) the increase of the strain ductility capacity of the anchorage (for example as a result of longer

anchorage length) results in higher relative drift ratio. This is secured by increasing the confinement level (from $a \cdot \omega_{wd}$ = 0.3 to 0.4, see the pink dashed lines in Fig. 5a).

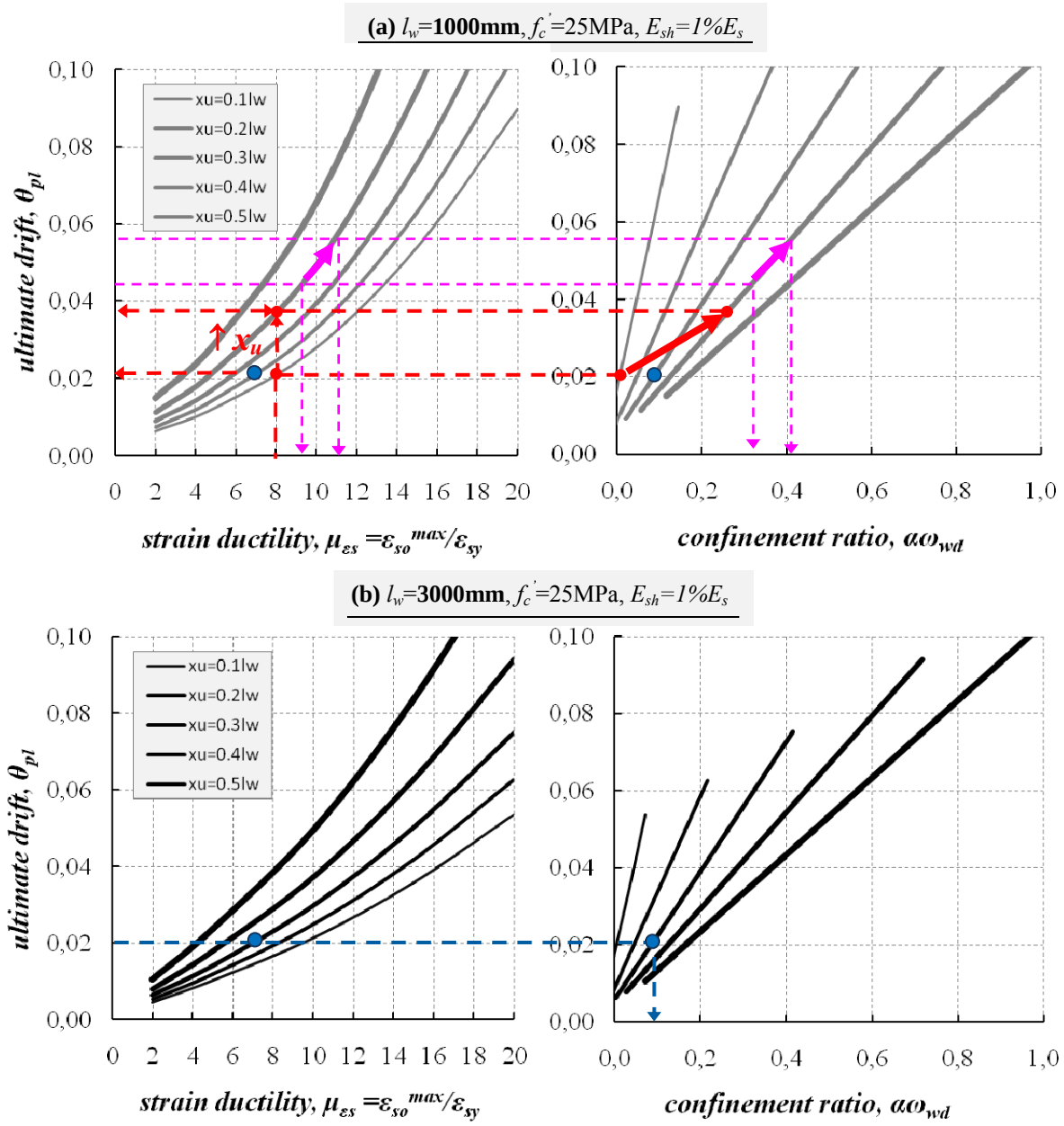

Figure 5. Design charts that correlate the ultimate drift of a wall with the strain ductility capacity of the anchorage and the confinement reinforcement ratio for wall section heights (a) l_w=**1000mm** and (b) l_w=**3000mm**. (Note that the anchorage properties were taken from Fig. 4b for steel **S500** with E_{sh}=1%E_s and concrete strength f_c'=25MPa.)

(ii) For the same strain ductility capacity of the anchorage (e.g. here, $\mu_{\varepsilon s}$=8, which is independent to the wall geometry, and it only depends on the anchorage detailing, i.e., for constant embedded length and good bond conditions), increasing the compression depth x_u from 0.1 to 0.4l_w results in a to higher demand of confinement reinforcement which in turn improves the ultimate drift capacity of the wall (see the red dashed lines in Fig. 5a).

(iii) Comparing the diagrams of Fig. 5 (a) and (b) in order to establish the effect of cross section height l_w, for the same ultimate drift ratio (i.e. 2%, blue dot in Fig. 5) and a strain ductility capacity of the anchorage ($\mu_{\varepsilon s}$=7) it is evident that the shorter element, for compression zone depth of x_u=0.2l_w, would require as confinement a transverse reinforcement ratio $a \cdot \omega_{wd}$ =0.1. To accomplish these

requirements with the longer wall element, the compression zone would have to extend over x_u=0.3l_w (see the blue dots in Fig. 5).

PRACTICAL IMPLICATIONS OF YIELD PENETRATION – A DESIGN EXAMPLE OF A SLENDER SHEAR WALL

Consider a seven-storey wall structure or a total height of H=21m, where the expected distance to the point of moment reversal is h_w=2/3H=14m from the base (Fig. 6a). The wall length is, l_w=3m, and wall thickness is b_w=300mm (thus b_o=250mm). The axial load ratio is v=0.1. Material properties for concrete and steel are, f_c=25MPa, f_{sy}=500MPa, respectively, with ε_{sy}=0.0025, E_{sh}=1%E_s. The wall is reinforced in the end zones with longitudinal bars having bars of diameter D_b=16mm provided with ample straight anchorage inside the footing (L_b/D_b=50). Setting the design behavior factor q equal to 3.5, it follows from Eq. 1 that the required curvature ductility at the critical section is μ_ϕ=6. If the reinforcement ratio of vertical web bars in the wall is ρ_v=0.002 (resulting in a mechanical reinforcement ratio of ω_v=0.04) the lower required value of the mechanical confining reinforcement ratio, $a\cdot\omega_{wd}$, is equal to 0.0406 (by implementing Eq. 2). In this case the strain of the extreme confined concrete fiber is $\varepsilon_{cc,u}$=0.00756 (by implementing Eq. 3). For Type I elastic response spectrum (where a_g=0.36g, with g=9.81m/sec^2), for ground type B (thus S=1.2, T_B=0.15sec, T_C=0.5sec and T_D=2sec) and period of an equivalent linear single-degree-of-freedom system $T=0.05\cdot H^{3/4}$=0.49sec, the resultant elastic spectral acceleration demand is $S_a=a_g\cdot S\cdot 2.5=0.36g\cdot 1.2\cdot 2.5$ thus S_a=1.08g and the corresponding elastic displacement is $S_d=S_a\cdot T^2/(4\pi^2)$=0.065m; thus the top elastic displacement of the wall is set to $\Delta_{el}=1.3\cdot S_d$=0.084m. By assuming equal energy absorption rule the resultant top plastic displacement of the wall is $\Delta_u=\Delta_{el}\cdot q/(2q-1)^{0.5}$=0.12m thus the plastic rotation is $\theta_{pl}=\Delta_u/15m$=0.57% (that is, lower than the minimum value θ_{pl}^{min}=0.7% defined by ACI 318, Chapter 21). Considering as plastic hinge length h_{cr}=0.3l_w=900mm, implementation of Eq. (4) results in x_u=1190mm and $x_{u,lim}$=551mm, thus the boundary element length in each side of the section wall is $l_c=x_u-x_{u,lim}\cong$640mm (greater than the code limit of max[0.15l_w,1.5b_w]=450mm). The associated tensile strain demand of the longitudinal bars is $\varepsilon_{so}=\varepsilon_{cc,u}(d_w-x_u)/x_u$=0.008 (it has been assumed that d_w=0.8l_w).

The implications of yield penetration on the above analysis are now examined by using the charts of Fig. 6b. Considering the anchorage geometry and the given values for the material strengths, for L_b/D_b=50 the strain ductility capacity of the anchorage is $\mu_{\varepsilon s}=\varepsilon_{so}^{max}/\varepsilon_{sy}$=14 thus ε_{so}^{max}=0.035 and s_o^{max}/D_b=0.4 thus s_o^{max}=6.4mm. However, to account for the tensile strain demand of ε_{so}=0.008, which corresponds to the compression strain $\varepsilon_{cc,u}$=0.00756 (in this case $\mu_{\varepsilon s}=\varepsilon_{so}/\varepsilon_{sy}$=3), the effective anchorage is treated as being shorter (L_b/D_b=32, blue dashed line in the left diagram of Fig. 6b); in this case the attained slip is defined as $s_o^{max}\approx 0.07D_b$=1.1mm. Based on the proposed model this amount of slip of the tension reinforcement imposes extra compression strain in the compressed zone of the section; implementing Eq. (5) the total compression strain is $\varepsilon_{cc,u}$=0.0088 whereas the initial plastic rotation θ_{pl}=0.57% is increased through Eq. (8a) to the value of 0.69% (the use of Eq. (8b) results in θ_{pl}=0.76%). For θ_{pl}=0.69% it is $x_{u,lim}$=455mm (it was 551mm), x_u=1141mm (it was 1190mm) whereas the boundary element length in each side of the section wall is increased from 640mm to $l_c=x_u-x_{u,lim}\approx$685mm.

The compression strain increase by 16% underscore the significance of confinement to avoid web toe crushing – a phenomenon often cited in post-earthquake reconnaissance reports – as well as in wall experimental studies. Clearly, accounting for the anchorage behavior in terms of attained slip at post-yield tensile strain demand, the boundary element geometry and confinement requirements are re-defined in order to provide the necessary resistance both to the lumped rotation due to pullout and to the increased compression strain of the wall cross section.

A notable point that is also relevant is the observation that the design code with the performance based requirement for boundary element definition appears pre-occupied with the strain magnitudes inside the confined part of the compression zone, thereby accepting that the cover will be delaminated at the toe, for the performance level considered. But recent studies suggest that additional measures such as externally bonded FRP layers wrapped locally around the toe and anchored over the length of

the boundary element will preclude cover delamination thereby eliminating even this occurrence of damage (Fardis et al., 2013).

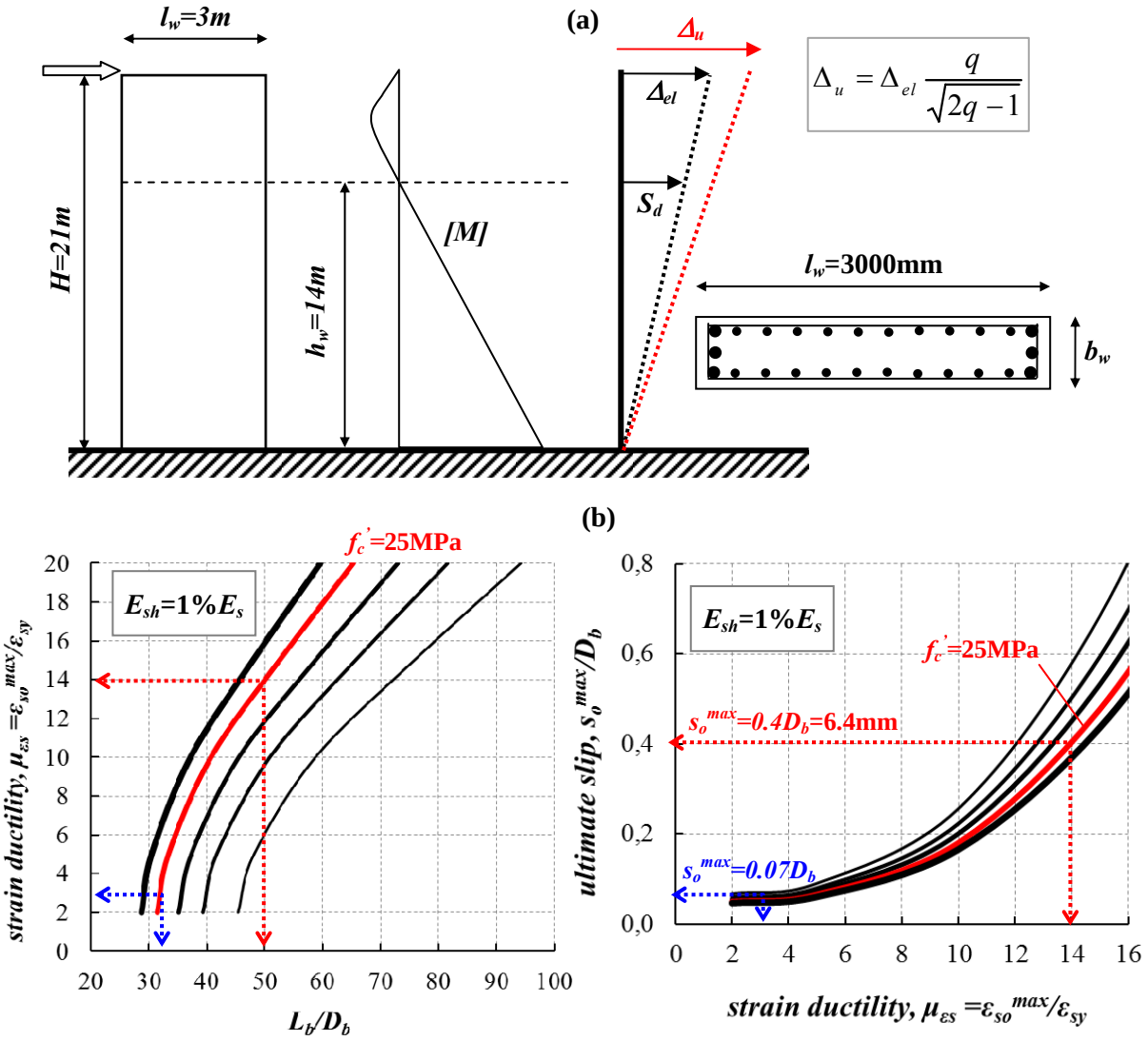

Figure 6. a) Geometry of the example wall and b) the use of the anchorage detailing charts for the definition of its strain capacity and the associated slip at the critical cross section of the wall.

CONCLUSIONS

Pullout rotation at the base of walls undergoing large lateral drifts due to yield penetration effectively increases the magnitude of compression strains and the extent over the wall length where boundary element confinement should be provided, the most critical being the ends where cover delamination is unavoidable in the absence of pertinent external confinement. An algorithm was developed to evaluate this effect. In deriving the underlying mechanistic model it was assumed that compression zone contraction owing to pullout rotation of tension steel affects the plastic hinge length, which, for the purposes of the analysis is taken equal to half the wall length; this assumption should be further studied through correlation with experimental data, with particular reference to the penetration of yielding into the region above the base. The effect studied would be accentuated significantly should this strain amplification be taken to occur over an even shorter plastic hinge length. Although many other phenomena may be also responsible for the observed crushing failures in structural walls during recent earthquakes (Wallace and Moehle 2012, Wallace et al. 2012) such as lateral buckling

due to out of plane displacements and second order effects, the importance of flexure-slip interaction should not be overlooked in light of the significant pullout slip values owing to yield-penetration, particularly if shorter anchorages / lap-splices or less favorable bond conditions prevail in field examples. Note here that the effect studied is also expected to overstrain longitudinal reinforcement in the compression zone of the wall base cross section, leading to the symmetric buckling patterns that were observed in field reconnaissance reports, such as that depicted in Fig. 2(c).

REFERENCES

ACI 318 (2011) Building Code Requirements for Structural Concrete (ACI 318M-11) and Commentary. American Concrete Institute, Farmington Hills, U.S.A. ISBN 978-0-87031-745-3

Eurocode 2 (EC2) (2004) BS EN 1992-1-1: Design of concrete structures—General rules and rules for buildings. European Committee for Standardization (CEN), Brussels.

Eurocode 8 (EC8-I) (2004) Design of structures for earthquake resistance – Part 1: General rules seismic actions and rules for buildings. European Committee for Standardization (CEN), Brussels.

Fardis M.N., Schetakis A., Strepelias E. (2013) "RC buildings retrofitted by converting frame bays into RC walls," *Springer Bull Earthquake Engineering*, 11:1541–1561.

fib CEB-FIP (2010) fib Model Code 2010 - Final draft, Volume 1. Bulletin No. 65, International Federation for Structural Concrete, Lausanne, Switzerland.

Hannewald P, Beyer K and Mihaylov B (2012) "Performance based assessment of existing bridges with wall type piers and structural deficiencies", *presented in the ACI341 Session: "Forming a Framework for Performance based Seismic Design of Concrete Bridges"*, *ACI Fall Convention*, Toronto, Canada.

Jiang H., Wang B., Lu X. (2013), "Experimental study on damage behavior of reinforced concrete shear walls subjected to cyclic loads," *Journal of Earthquake Engineering*, Taylor and Francis, 17:958–971.

Karagiannis Chr. (2013). Design, Response of Reinforced Concrete Structures against earthquakes, Editor. Sofia A.E., ISBN 978-960-6706-66-0, pp. 584.

Syntzirma, D., Pantazopoulou, S., and Aschheim, M. (2010). "Load-history effects on deformation capacity of flexural members limited by bar buckling*," ASCE Journal of Structural Engineering*, 136(1):1–11.

Tastani S.P. and Pantazopoulou S.J. (2013). "Yield penetration in seismically loaded anchorages: effects on member deformation capacity," *Techno press Earthquake and Structures*, 5(5):527-552

Wallace JW and Moehle J (2012) "Behavior and design of structural walls – Lessons from recent laboratory tests and earthquakes", *Proceedings of the Int. Symposium on Engineering Lessons learned from the 2011 Great East Japan Earthquake*, Tokyo, Japan, 1-4March, 1132-1144.

Wallace JW, Massone LM, Bonelli P, Dragovich J, Lagos R, Lüders C, and Moehle J (2012) "Damage and implications for seismic design of RC structural wall buildings," *Earthquake Spectra*, 28(1):281-299.